Raman Enhancement Factor of a Single Tunable Nanoplasmonic Resonator

Kai-Hung Su, Stéphane Durant, Jennifer M. Steele, Yi Xiong, Cheng Sun, and Xiang Zhang*

5130 Etcheverry Hall, NSF Nanoscale Science and Engineering Center (NSEC), University of California, Berkeley, California 94720-1740

Received: September 29, 2005; In Final Form: December 30, 2005

We have developed a novel technique to precisely determine the Raman enhancement factor in single nanoplasmonic resonators (TNPRs). TNPRs are lithographically defined metallodielectric nanoparticles composed of two silver disks stacked vertically, separated by a silica layer. At resonance, the local electromagnetic fields are enhanced at the TNPR surface, making it an ideal surface-enhanced Raman scattering (SERS) active substrate. The ability to control the dimensions of the metallic and dielectric layers offers the unique advantage of fine-tuning the plasmon resonance frequency to maximize the enhancement of the Raman signal. Furthermore, by selective shielding of the outer surface of the metallic structure, the efficiency can be further enhanced by guiding the molecular assembly to the locations that exhibit strong electromagnetic fields. We experimentally demonstrate SERS enhancement factors of $(6.1 \pm 0.3) \times 10^{10}$, with the highest enhancement factor being achieved by using an individual nanoparticle. By using nanofabrication techniques, we eliminate the issues such as large size variations, cluster aggregation, and interparticle effects common in preparing SERS substrates using conventional chemical synthesis or batch fabrication methods. TNPRs produce very controllable and repeatable SERS signals at the desired locations and, thus, make an ideal candidate for device integration.

Introduction

Raman spectroscopy provides a label-free technique for the detection of molecules by detecting their distinct signature of vibrational modes. However, Raman scattering has an extremely small cross section and, for practical applications, Raman signals must be significantly enhanced. Recently, researchers have utilized the strong local and scattered fields associated with the plasmon resonance of noble metal nanoparticles to enhance Raman signals.[1−5] The surface plasmon resonance occurs when the frequency of the incident light excites a collective oscillation of conduction electrons which induce strong local and scattered fields. The Raman intensity scattered by a molecule located within this enhanced electromagnetic field can be greatly amplified by several orders of magnitude, an effect termed surface-enhanced Raman scattering (SERS).

The early developments of SERS involved using aggregated colloids that had so-called "hot spots" at the junction of two or more particles where the electromagnetic field is strongly enhanced. The enhancement factor (EF) of these hot spots can reach 10^{14}.[2,3] However, due to the stochastic nature of nanoparticle aggregation, it is difficult to reliably reproduce the hot spots at the specific location. For practical applications, it is imperative to develop SERS active substrates with reproducible and controllable SERS enhancements. Therefore, recent research has concentrated on highly ordered metallic nanostructure systems because their optical properties can be better controlled via state-of-the-art nanofabrication methods. Several research groups have experimentally demonstrated well-defined plasmon resonances by precise fabrication of nanoparticles such as triangles,[6] nanoshells,[7] nanoprisms,[8] nanorings,[9] nanophotonic crescents,[10] nanoplasmonic resonators,[11] and one-dimensional nanoparticle chains.[12]

Previously, we reported on multilayered nanoparticles consisting of alternating metal and dielectric disks, known as tunable nanoplasmonic resonators (TNPRs), which exhibit a tunable plasmon resonance giving rise to a host of applications.[13] The ability to individually tune the dimensions of the metallic and dielectric layers offers the unique advantage of maximizing the enhancement by fine-tuning the resonance to match the Raman pump wavelength.[14] In addition, TNPR nanofabrication methods provide a well-controlled process to reliably produce optimal SERS enhancement at the desired location on the substrate.

In this report, we present a quantitative study of the SERS enhancement factor (EF) of TNPRs. By direct comparison to the Raman spectrum for the nonenhanced case, the SERS EF for an individual TNPR can reach $(6.1 \pm 0.3) \times 10^{10}$. The nanofabrication method also allows an additional SiO_2 cap layer to be fabricated on top of TNPRs. This layer prevents Raman dye molecules from assembling on the top TNPR surface and, thus, isolates the SERS signal contributed by the molecules assembled on the sidewall of the TNPR. Theoretical surface plots of the electromagnetic field, at resonance, indicate that the electromagnetic enhancement at the sidewalls of the TNPRs is greater than that at the top surface. By comparing the SERS signals measured from TNPRs with different structures, one can determine the SERS EF originating from the sidewalls and top surface. These results help us to understand the SERS enhancement contribution at the TNPR surface.

Experiment

The TNPRs were patterned on quartz substrates (HOYA Co.) by electron beam lithography (EBL) (Leica Microsystems Nanowriter Series EBL 100). A 30 nm thick indium tin oxide (ITO) layer was first sputtered on the substrate to prevent charging effects during the EBL process. Poly(methyl methacrylate) (100 nm thick, MicroChem Corp. PMMA) films, spin-

---

* Corresponding author. E-mail: xiang@berkeley.edu.

Raman Enhancement Factor of TNPRs

J. Phys. Chem. B, Vol. 110, No. 9, 2006 **3965**

SCHEME 1: Schematic Drawing of a TNPR (a) and a Capped TNPR (b) before and after the *p*-Mercaptoaniline (*p*MA) Self-Assembled on the Metal Surface[a]
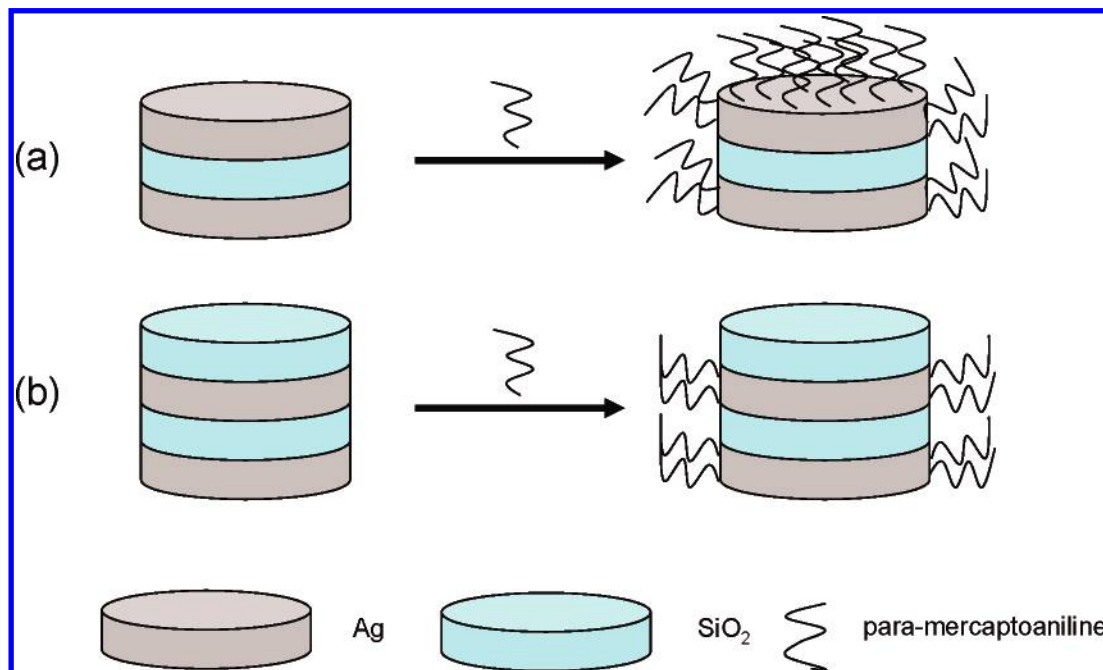
[a] The sandwiched SiO_2 layer works as a tuning parameter for plasmon resonant frequency, while the top SiO_2 layer works as a capping layer to prevent the molecules from self-assembling on the top metal surface.

coated on the ITO-quartz glass, were used as a positive photoresist. After exposure, the patterns were developed using a 1:3 ratio of a methyl isobutyl ketone and isopropyl alcohol mixture, followed by multilayer electron beam evaporation of silver and oxide and standard lift-off procedures. We fabricated three-layered $Ag/SiO_2/Ag$ and four-layered $Ag/SiO_2/Ag/SiO_2$ TNPRs on the same substrate (we refer to the four-layered TNPR as the capped TNPR in this paper), with each silver and SiO_2 layer thickness fixed at 20 and 5 nm, respectively (Scheme 1). A shadow mask was inserted over the three-layered TNPRs during deposition of the additional 5 nm SiO_2 capping layer to prevent deposition on the three-layered TNPRs. The samples were measured by scanning electron microscopy and atomic force microscopy to determine their sizes, shapes, and thicknesses. The SiO_2 layer sandwiched between the metallic layers can be used to tune the surface plasmon resonance frequency by adjusting its thickness. The EF can be maximized by matching the surface plasmon resonance to the pump laser frequency.[14,15] Under an optical microscope, these particles, as shown in Figure 1a, are distinctively visible due to the strong scattering of light at resonant wavelengths. Scanning electron microscopy (SEM) images (Figure 1b) show that the TNPRs are slightly elongated with a long axis and short axis of 117 and 81 nm, respectively. Atomic force microscopy (AFM) measurement (Figure 1c) confirms that the height difference between capped TNPRs and noncapped TNPRs is 5 nm, which matches the thickness of the SiO_2 capping layer. Conducting AFM was used to ensure a good SiO_2 layer coverage between the metal disks.[13]

Scattering spectra were obtained by illuminating the TNPRs with collimated light delivered by a multimode optical fiber from a 150 W Xe white light source. The light was delivered through a right angle prism at an angle resulting in total internal reflection (TIR), and the scattered light was collected with a JY (550 grating) spectrometer system (Jobin Yvon).[16] For the SERS experiment, SERS spectra were measured using a modified Zeiss inverted confocal microscope with a 20×

objective in a backscattering geometry. An argon laser operating at 514 nm (attenuated to ~10 mW) was coupled into the microscope, and the appropriate interference filters and holographic notch filter (Kaiser) were placed in the beam path to remove the unwanted laser lines. The output light path was coupled into the same spectroscope as the scattering spectra measurement.

Results and Discussion

Measured scattering spectra of TNPRs are showed in Figure 2. In the measurements, the polarization of the incident *E*-field is parallel to the TNPR long axis. Figure 2a depicts the scattering spectra of an individual TNPR and a capped TNPR with resonant peaks at 516 and 536 nm, respectively. The sandwiched SiO_2 layer works as a tunable coupling factor for the plasmon resonant frequency, and the top SiO_2 layer works as a cover layer to prevent the molecules from self-assembling on top of the metal surface. The observed red-shift of the resonance spectrum of the capped TNPR is due to the presence of the SiO_2 layer, which locally increases the refractive index.[17] *p*-Mercaptoaniline (*p*MA), a commonly used Raman dye, was selected in this study.[18,19] The low fluorescence emission background makes it a good candidate for qualitative analysis of the Raman signal. To ensure maximum coverage of the *p*MA monolayer on the TNPR surface, the substrates were incubated in a 100 μM *p*MA solution for more than 24 h. After repeatedly rinsing with DI water to remove unwanted *p*MA adsorbed on the substrate and SiO_2 capping layer, the substrate was thoroughly dried with N_2 gas. The spectra measurements indicate the scattering peak positions of *p*MA-coated capped and noncapped TNPRs were shifted to 534 and 550 nm, respectively (Figure 2b). The results indicate that the presence of *p*MA in the vicinity of the TNPR causes a red-shift of the resonance spectrum, equaling 18 nm for noncapped TNPRs and 14 nm for capped TNPRs. This observation shows that *p*MA on top of an uncapped TNPR does not lead to a significant shift (below
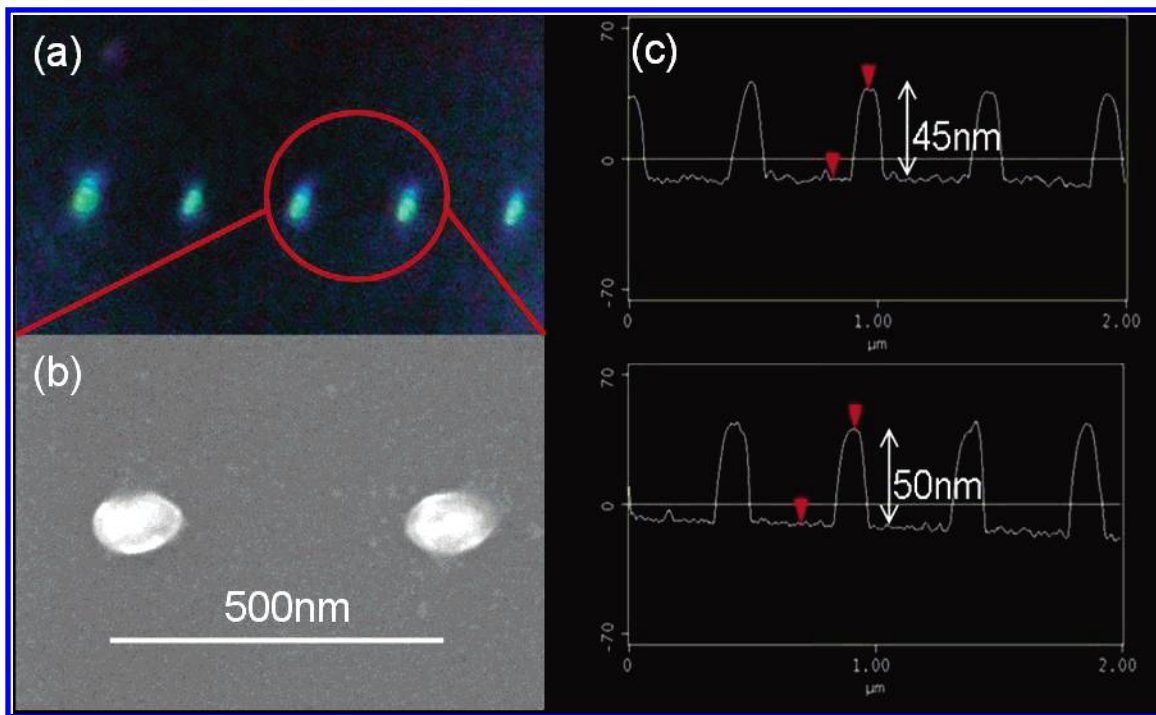
Figure 1. (a) Real color picture of TNPRs illuminated by evanescent white light waves taken with a digital camera. (b) SEM image of a Au/ SiO$_2$/Au three-layered TNPR singlet. (c) AFM measurement of a TNPR and a 5 nm SiO$_2$-capped TNPR. The measured height difference shows that a 5 nm SiO$_2$ layer was successfully deposited on top of the metal surface while a shadow mask was inserted over the TNPR to prevent SiO$_2$ layer deposition.

5 nm) and the surface plasmon modes in the TNPR may be more sensitive to the local refractive index change on the sidewall (in the direction of the excitation electric field) than on the top surface. Numerical simulations are more desirable to obtain a qualitative explanation of the peak shift for different sample configurations. It should be noted that these peak shifts suggest TNPRs can also serve as molecule/bio sensors to monitor local refractive index changes.[20,21]

The SERS EF for the TNPRs was evaluated by directly comparing the SERS intensity obtained from TNPRs with unenhanced molecules using the expression EF = (RS^{TNPR}/ RS^{reference})([reference]/[TNPR]). RS^{TNPR} and RS^{reference} are the measured SERS intensity of the TNPRs and normal Raman standard sample, respectively. [TNPR] and [reference] are the estimated number of molecules in the experiments. A saturated *p*MA monolayer coverage of 0.39 nm^2 per molecule is used to estimate the number of molecules on a TNPR surface.[18] Assuming that an individual TNPR is a cylindrical ellipsoid particle, the maximum number of *p*MA molecules that can self-assemble is $\sim$5.1 × 10^4. A 0.1 mL neat liquid *p*MA (1.06 g/cm^3) droplet on a quartz substrate with a known detection volume from a 20× microscope objective was used to estimate the number of molecules for the reference sample, giving $\sim$4.5 × 10^{13} *p*MA molecules.[22] We took SERS spectra on a single TNPR at 10 different locations with exactly the same exposure time and individual Raman spectra, which are depicted in Figure 3. Remarkably, the intensities of the measured Raman spectra are very constant, showing that fabrication repeatability of particles shapes is very reliable. Especially, the signal strengths of the 1590 and 1077 cm^{-1} ring modes of *p*MA were monitored. By looking carefully at the raw data, we found that the intensity of these two modes is very constant among measurements. The maximum SERS EF from an individual TNPR reached $\sim$(3.4 ± 0.3) × 10^{10} and (2.9 ± 0.3) × 10^{10} at 1077 and 1590 cm^{-1}, respectively, and the error bars were obtained from sample-to-sample variation of Raman scattering intensity. It should be

noted that the possible error in estimating the surface coverage of *p*MA and the volume illuminated by the microscope objective obviously affects the precision in calculating the SERS EF. To provide a trustworthy estimation of the SERS EF for a TNPR, we are performing the calculation in the most conservative manner. The SERS EF was determined by assuming maximum *p*MA coverage over the entire TNPR metal surface and with the smallest volume being illuminated by microscope objectives. The reported value is in fact representing the lower bound of the SERS EF, and the actual EF can be even higher.

We also measured the Raman spectra on SiO$_2$-capped TNPRs to isolate the SERS contribution from the sidewall of the capped TNPRs. We assumed that there are no *p*MA molecules self-assembled on the SiO$_2$ layer after copious DI water rinsing. The ratio of *p*MA molecules self-assembled on the exposed metal surface of the TNPR to that of the capped TNPR was assumed to be the same as the area ratio, which is about 1.6. The maximum measured SERS EF intensity on the capped TNPR reaches (6.1 ± 0.3) × 10^{10} and (4.6 ± 0.3) × 10^{10} for the 1077 and 1590 cm^{-1} ring modes, respectively. The relative SERS intensity ratio for a TNPR to a capped TNPR is approximately 1.3. This is an interesting observation, since the SERS EF ratio between the capped TNPR and the TNPR is not proportional to the number of molecules assembled on the exposed metal surface.

To understand these experimental results, we performed several numerical calculations. We applied the discrete dipole approximation (DDA) method to compute the near field distribution of the *E*-field surrounding the TNPR.[23,24] Figure 4 shows the calculated *E*-field amplitude distribution at the sidewall and top surface of a TNPR with the geometrical parameters corresponding to the SEM and AFM measurements. The permittivity of Ag is taken from the literature for bulk Ag material,[25] and the permittivity of SiO$_2$ is set to 2.13. The substrate, which has significant effects on the plasmon reso-nance,[17] is taken into account by embedding the particle in a

Raman Enhancement Factor of TNPRs
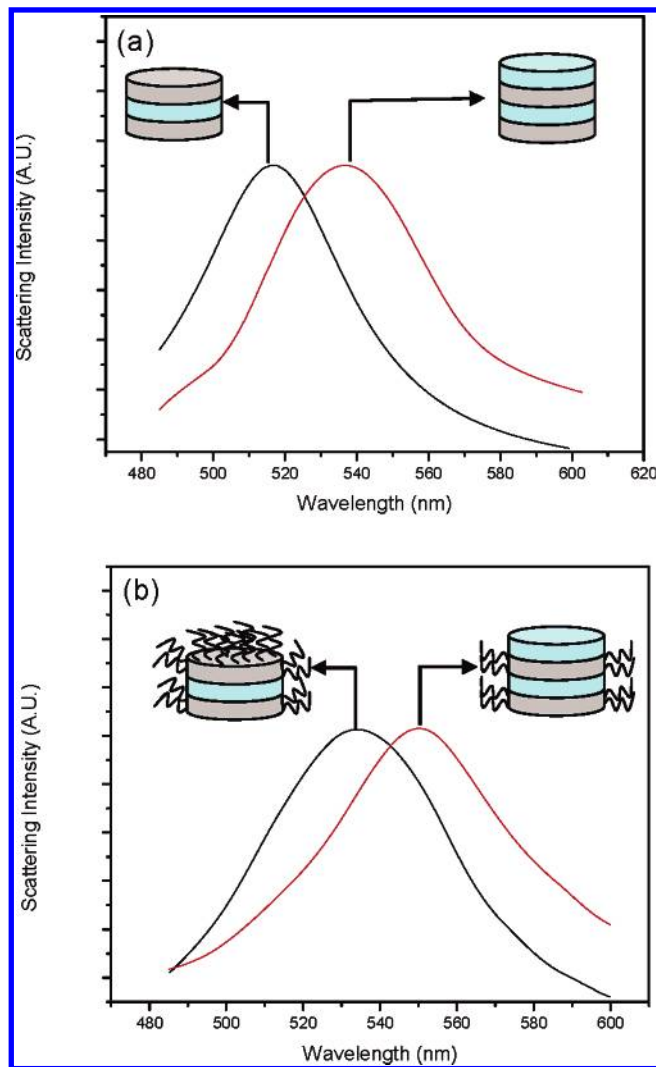
J. Phys. Chem. B, Vol. 110, No. 9, 2006 **3967**

Figure 2. (a) Measured scattering spectra for an individual TNPR and a capped TNPR before *p*MA incubation. The Ag and SiO$_2$ layer thicknesses are 20 and 5 nm, respectively. (b) Measured scattering spectra for an individual TNPR and a capped TNPR after 100 μM *p*MA incubation for 24 h. The curves were normalized such that the maximum peak positions are identical.
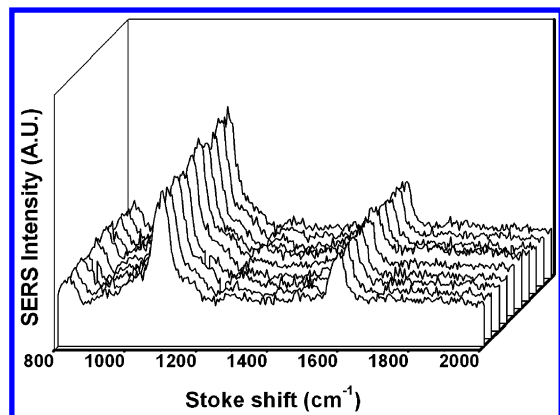

Figure 3. Ten surface-enhanced Raman spectra of *p*MA measured on different individual TNPRs. The integration time for each Raman spectrum is 30 s. Results are plotted without normalization.

homogeneous medium with a refractive index of 1.4, which is the averaged refractive index of air and ITO.[26] Figure 4a clearly shows an angular dipole-like *E*-field distribution where stronger fields are localized along the incident polarization direction θ = 0 (along the TNPR long axis). The z dependence of the field
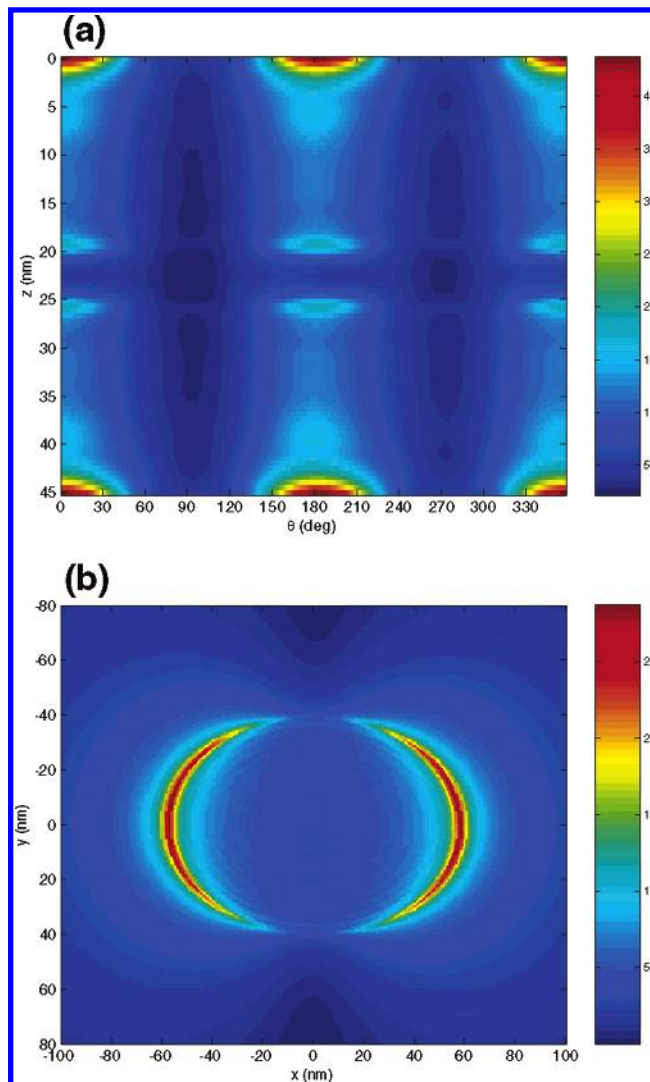

Figure 4. (a) Amplitude distribution of the total field computed just outside the side of the curved cylindrical surface. (b) Amplitude distribution of the total field computed above the top TNPR metal surface.

shows that the strong local fields are mainly distributed close to the Ag/SiO$_2$, Ag/air, and Ag/ITO interfaces. Figure 4b shows that the stronger fields or "hotter spots" are mainly located close to the edge of the ellipse around the direction of the incident polarization.

The Raman intensity scattered by each molecule is known to be proportional to the fourth power of the local amplitude of the electromagnetic field.[2] By assuming that a homogeneous distribution of molecules are attached to the TNPR surface boundary, the SERS intensity reported in the experiment should be proportional to the quantity S_T, defined by $\int_{V_T} |E/E_0|^4 \, dv$, where V_T is the volume occupied by biomolecules surrounding the TNPR. The calculated S_T (μm^3) values for the sidewall surface and the top flat surface are 0.1973 and 0.0507, respectively, indicating 80% of the overall signal is contributed from the sidewall. This result is also in good agreement with the experimentally measured SERS intensity ratio of 1.3 between the uncapped TNPR, for which SERS occurs on both sidewalls and the top surface, and the SiO$_2$-capped TNPR, for which SERS occurs only on the sidewalls.

Conclusions

In summary, we studied the SERS EF of TNPRs. The observed SERS EF of a single TNPR can be as large as 6.1 $\times$

10^{10} when the plasmon resonance is tuned to the pump laser frequency, which is among the highest reported to date. We developed a novel technique that forces the molecules to be assembled on the sidewall of the resonator where the field is strongest, giving an accurate measurement of the Raman enhancement factor. The experimental results agree well with numerical calculations of the TNPR. Nanofabrication enables precise dimension control and accurate placement of the TNPRs, eliminating the issues resulting from aggregation and size variation effects, often associated with chemical synthesis or self-assembly of colloidal nanoparticles. Thus, it offers a unique advantage for the development of integrated biosensing devices.

References and Notes

(1) Kreibig, U.; Vollmer, M. *Optical Properties of Metal Clusters*; Springer-Verlag: Berlin, 1995.

(2) Kneipp, K.; Wang, Y.; Kneipp, H.; Perelman, L. T.; Itzkan, I.; Dasari, R. R.; Feld, M. S. *Phys. Rev. Lett.* **1997**, *78*, 1667.

(3) Nie, S.; Emory, S. R. *Science* **1997**, *275*, 1102.

(4) Xu, H. X.; Bjerneld, E. J.; Käll, M.; Börjesson, L. *Phys. Rev. Lett.* **1999**, *83*, 4357.

(5) Lin, H.; Mock, J. J.; Smith, D. R.; Gao, T.; Sailor, M. J. *J. Phys. Chem. B* **2004**, *108*, 11654.

(6) Haynes, C. L.; Van Duyne, R. P. *J. Phys. Chem. B* **2003**, *107*, 7426.

(7) Jackson, J. B.; Westcott, S. L.; Hirsch, L. R.; West, J. L.; Halas, N. J. *Appl. Phys. Lett.* **2003**, *82*, 257.

(8) Jin, R. C.; Cao, Y. W.; Mirkin, C. A.; Kelly, K. L.; Schatz, G. C.; Zheng, J. G. *Science* **2001**, *294*, 1901.

(9) Aizpurua, J.; Hanarp, P.; Sutherland, D. S.; Käll, M.; Bryant, G. W.; García de Abajo, F. J. *Phys. Rev. Lett.* **2003**, *90*, 057401.

(10) Lu, Y.; Liu, G. L.; Kim, J.; Mejia, Y. X.; Lee, L. P. *Nano Lett.* **2005**, *5*, 119.

(11) Wei, Q.; Su, K. H.; Zhang, X. X.; Zhang, X. *Proc. SPIE* **2003**, *5221*, 92.

(12) Wei, Q.; Su, K. H.; Durant, S.; Zhang, X. *Nano Lett.* **2004**, *4*, 1067.

(13) Su, K. H.; Wei, Q.; Zhang, X. *Appl. Phys. Lett.* **2006**, accepted for publication.

(14) Jackson, J. B.; Halas, N. J. *Proc. Natl. Acad. Sci. U.S.A.* **2004**, *101*, 17930.

(15) McFarland, A. D.; Young, M. A.; Dieringer, J. A.; Van Duyne, R. P. *J. Phys. Chem. B* **2005**, *109*, 11279.

(16) Su, K. H.; Wei, Q.; Mock, J. J.; Smith, D. R.; Zhang, X. *Nano Lett.* **2003**, *3*, 1807.

(17) Malinsky, M. D.; Kelly, K. L.; Schatz, G. C.; Van Duyne, R. P. *J. Phys. Chem. B* **2001**, *105*, 2343.

(18) Mohri, N.; Matsushita, S.; Inoue, M. *Langmuir* **1998**, *14*, 2343.

(19) Osawa, M.; Matsuda, N.; Yoshii, K.; Uchida, I. *J. Phys. Chem.* **1994**, *98*, 12702.

(20) McFarland, A. D.; Van Duyne, R. P. *Nano Lett.* **2003**, *3*, 1057.

(21) Mock, J. J.; Smith, D. R.; Schultz, S. *Nano Lett.* **2003**, *3*, 485

(22) Nie, S.; Zare, R. N. *Ann. Rev. Biophys. Biomol. Struct.* **1997**, *26*, 567.

(23) Draine, B. T.; Flatau, P. J. *J. Opt. Soc. Am. A* **1973**, *11*, 1491. Draine, B. T.; Flatau, P. J. User Guide to the Discrete Dipole Approximation Code DSCAT.6.0. http://arxiv.org/abs/astro-ph/0300969 (accessed 2003).

(24) Jesen, T.; Kelly, L.; Lazarides, A.; Schatz, G. C. *J. Cluster Sci.* **1999**, *10*, 295. Felidj, N.; Aubard, J.; Levi, G. *J. Chem. Phys.* **1999**, *111*, 1195.

(25) Johnson, P. B.; Christy, R. W. *Phys. Rev. B* **1972**, *6*, 470.

(26) Tamaru, H.; Kuwata, H.; Miyazaki, H.; Miyano, K. *Appl. Phys. Lett.* **2002**, *80*, 1826.